

Two-photon axonal calcium imaging of the claustrum in behaving mice

Candidate 1030338



Word Count: 6,551

August 14th 2019

Presented for the degree of
MSc in Neuroscience

Contents

1	Introduction	4
2	Methods	7
2.1	Animals	7
2.2	Stereotaxic surgery	7
2.3	CTB labelling of CLA projection neurons	9
2.4	GCaMP delivery to CLA	9
2.5	Chronic window implantation	9
2.6	Histology	10
2.7	Steering wheel task set-up	10
2.8	Training in the steering wheel task	11
2.9	Whisker stimulation	14
2.10	Two-photon imaging in the awake mouse	14
2.11	Axonal calcium imaging analysis	15
3	Results	17
3.1	Projection-defined CLA neurons	17
3.2	A behavioural scenario to probe the CLA	19
3.3	Imaging during the steering wheel task	21
3.4	CLA axonal responses to somatosensory stimulation	22
4	Discussion	26
5	References	29

Acknowledgements

I would like to thank all members of the Packer lab for their help during the project, both when experiments worked and when they did not. Special thanks to Andrew Shelton for teaching me how to do surgeries and for being an endless wealth of information on everything one would ever want to know about the claustrum. Also, I would like to acknowledge David Oliver for his help and advice during the project, Hamish Forrest for sharing his wisdom on what relates to animal behaviour, Jimmy Rowland for help with code and doctors Rob Lees and Adam Packer for their help with two-photon microscopy — and in addition, to the later for his supervision.

Author contribution

Cranial window implantations and GCaMP injections were made by Dr. Adam Packer. Any other surgeries were made entirely by the candidate. The core code for managing the steering wheel task was provided by the Cortex Lab, UCL. Data was obtained and analysed by the candidate. The steering wheel set up was built and optimised by the candidate.

Abstract

Despite being first described more than two centuries ago, the function of a cortical nucleus known as the claustrum remains a mystery. Its pattern of extensive connectivity with many cortical areas has motivated the proposal that it may play a central role in cognitive function. However, its peculiar morphology, together with the fact that its borders are ill described — which is still a matter of debate — has prevented scientist from properly interrogating the claustrum. Nowadays molecular markers in combination with genetically encoded calcium indicators and opsins allow optical interrogation of brain circuits. However, once again the claustrum seems to escape these approaches as currently there is not a good genetic marker specific to this structure. Here we overcame this limitation by expressing a state of the art genetically encoded calcium indicator through a recently developed retrograde viral strategy. We trained mice in a novel sensory-guided task — the steering wheel task — and recorded *in vivo* the activity of single claustrum axons in the prefrontal cortex. In contrast to what we expected based on previous studies, we found no correlation between the activity of claustrocortical collaterals and the delivery of rewards or the presentation of visual stimuli during the task. However, this was a pilot study with a reduced cohort and numerous unforeseen technical limitations and problems, which prevented us from acquiring good quality data. Further studies using calcium imaging and optogenetics, either replicating this one in a larger number of animals or using other behavioural paradigms, may help clarify the role of the claustrum in cortical function.

1 Introduction

Deep in the neocortex lies an enigmatic grey matter structure with unknown function and singular connectivity: the claustrum (CLA). In primates, cats, rodents and other higher mammals the CLA is located medial to the insula, lateral to the striatum, and dorsal to the endopiriform nucleus (Johnson and Fenske, 2014). Intriguingly, this structure shows reciprocal ipsilateral and contralateral connectivity with most cortical areas and almost absent subcortical input (Pearson et al., 1982). It densely innervates orbitofrontal, anterior cingulate (ACA) and retrosplenial (RSC) cortices, and also collateralises extensively to associative and motor areas in the parietal lobe (Wang et al., 2017; Jackson et al., 2018; Zingg et al., 2018). CLA neurons are very heterogeneous in their projection targets with even a subset of them – mainly located in the caudal region – wrapping the entire neocortex (Wang et al., 2019). Because of their extensive axonal tree, the term ‘crown of thorns’ has been coined to describe such neurons. Also, it is the most highly connected structure per unit volume in the human brain (Fernández-Miranda et al., 2008; Torger-son et al., 2014). All this evidence situates the CLA in an ideal position for integrating cortical information and giving rise to conscious percept (Crick and Koch, 2005).

There are separate retinotopic (Kennedy and Bullier, 1985; LeVay and Sherk, 1981; Olson and Graybiel, 1980) and somatotopic maps in the CLA (Olson and Graybiel, 1980; Majak et al., 2002), as well as regions that respond exclusively to sound or to visual stimuli (Remedios et al., 2010). This, together with a myriad of histological studies in the CLA of several species has demarcated the existence of a rough topological map of the cortex in the CLA (but see Atlan et al. (2018) regarding a different view in rodents).

Because of its promiscuous connectivity, it is very difficult to assign a single role to the CLA. Over the years it has been implicated in a variety of different functions, ranging from multisensory integration (Olson and Graybiel, 1980) to top-down control (White et al., 2018b), but none of the studies has been conclusive in assigning a precise function. Recently, a number of research teams have implicated the CLA in saliency detection

and attention (Atlan et al., 2018; Bayat et al., 2018) as well as cognitive control (White et al., 2018a; Krimmel et al., 2019). A role for orchestrating sleep has also been probed, although this newly proposed function still lacks solid evidence (Renouard et al., 2015; Narikiyo et al., 2018).

One of the major drawbacks of functional studies investigating the CLA *in vivo* has been its lack of specificity. Classic recording techniques require a large study area, as opposed to CLA morphology which consists in a thin layer of cells (Mathur et al., 2009). *In vivo* electrophysiological studies have been criticised due to the difficulty to delineate whether recorded units belonged to the CLA or the nearby insular cortex, yielding contradictory results (Sherk, 2014). Also, the borders of the claustrum with other cortical areas and within clastral areas are poorly defined and appear to vary among species (Binks et al., 2019; Dillingham et al., 2019). There have been attempts to characterize and define molecular markers of the CLA (Watakabe et al., 2014), but the early success has been dampened by the finding that most of these markers produce off-target labelling in surrounding areas (Wang et al., 2017). So far, the most promising candidate seems to be VGLUT2, which is not expressed in near-by cortical areas such as the insula.

A newly developed adeno-associated virus (AAV) variant that travels retrogradely has opened the door to a different strategy to specifically label the CLA (Tervo et al., 2016). Retrograde labelling from orbitofrontal cortex, ACA and RSC labels the CLA with different degrees of specificity and to a different extent (Jackson et al., 2018; Zingg et al., 2018). In particular, retrograde labelling from the RSC has been claimed to be the most specific method so far. Specific targeting with viral strategies also allows us to deliver molecular tools with the objective of recording and manipulating CLA activity. Recently developed genetically encoded calcium indicators are optimal for *in vivo* recording of neural activity of a large population of neurons and can be delivered to brain tissue via viral transduction (Dana et al., 2018). Selectively expressing a calcium indicator in the CLA will allow to *in vivo* probe a variety of functions by recording a large number of neurons.

This study will investigate *in vivo* axonal responses of RSC-projecting CLA neurons in behaving mice and is divided into three specific aims:

- 1) To investigate the extent of overlap of RSC and ACA-projecting CLA neurons.
- 2) To build and make functional a steering wheel task set up.
- 3) To record and analyse how CLA collaterals respond during the task and during somatosensory stimulation.

2 Methods

2.1 Animals

All surgical procedures were carried out under license from the UK Home Office in accordance with the Animals (Scientific Procedures) Act 1986. Experiments were conducted on wildtype male mice with C57BI6/J background. Animals were housed on a 12 h light/dark cycle and given *ad libitum* access to water and food unless otherwise stated (see section 2.8 in page 11).

2.2 Stereotaxic surgery

Surgical procedures were performed under aseptic conditions and were optimised to cause the least stress or discomfort to the mice. The procedure started with induction of anaesthesia in a chamber prefilled with 5 % isoflurane dissolved in oxygen at a flow rate of 1 litre per minute, followed by shaving of the scalp. After induction, a face mask was used to deliver the anaesthetic at 1.5-2 % at 0.1-0.3 litres per minute. Animals were i.p. injected with Vetergesic (0.1 mg/kg) and Metacam (5 mg/kg) to achieve an appropriate level of analgesia. Pedal and tail pinch reflexes, as well as respiratory rate were used to asses level of anaesthesia and adjust anaesthetic delivery as appropriate to maintain surgical plane. At this point animals were head-fixed on a stereotaxic surgical rig with a built-in heater set to 35°C to maintain body temperature (Stoeling). Scalp around the surgical area was disinfected with sterile chlorhexidine (Chloraprep) and a small incision was opened along the midline. A local anaesthetic, Bupivacaine (Marcaine), was then gently applied under the scalp before removing the periosteum. Eyes were protected with a gel to prevent drying and protect the cornea (Viscotears). Skull was then levelled anterior to posterior and left to right to adjust the bregma-lambda axis relative to the stereotaxic frame. Then, one or several intracranial injections were made. In three mice, a chronic window and a head-plate were also implanted for *in vivo* imaging purposes.

Further details for these procedures are given in later sections.

To account for different brain sizes along postnatal development, stereotaxic coordinates were scaled by the measured bregma-lambda distance with respect to that in the Allen Reference mouse brain atlas (Goldowitz, 2010). Coordinates in the reference atlas were used guide the opening of a small hole – around 0.5 mm in diameter –with a mini-drill (NSX Volvere i7). In order to avoid damaging the brain during the drilling, once the skull was gently thinned forceps were used to remove the last piece of skull. The following coordinates were used: For injections in the RSC, 3 mm posterior and 0.5 mm lateral to bregma and 1 mm ventral from the cortical surface; For injections in the ACA, 0.5 mm anterior and 0.4 mm lateral to bregma and 0.9 mm ventral from the cortical surface. For injections in the CLA, 1 mm anterior and 3.4 mm lateral to bregma and 2.6 mm ventral from the cortical surface. Viruses or anatomical tracers were delivered into these locations at a rate of 50-100 nL/min through pulled glass micropipettes (Shutter Instruments P-1000) of around 20 micrometres of diameter in the tip prefilled with mineral oil and bevelled to a sharp point. The pipettes were connected to a micromanipulator controlling a hydraulic injector (Narshige).

A 5-minute wait was allowed just after the injection for the virus or tracer to diffuse. Then the pipette was withdrawn and the scalp was sutured with Monocryl. The animal was then placed on a recovery cage containing highly palatable food, autoclavable dust-free bedding, Metacam jelly and water bottles with longer spouts, along with standard enrichment material. Half of the recovery cage was placed over a heating pad to allow the animal to choose the temperature until signs of full motor recovery. Then the heating pad was removed. Animal appearance, behaviour and weight was monitored twice per day for the two first days and once per day the subsequent three to five days until full recovery. All animals were allowed to recover fully before further experimental procedures.

2.3 CTB labelling of CLA projection neurons

For anatomical studies, ten wild type mice were injected with 80 nL of cholera toxin subunit B (CTB) conjugated to an Alexa fluorophore (Alexa-487, Alexa-555 or Alexa-647, ThermoFisher) into the RSC and ACA in the right hemisphere. Different fluorophores were used in each of the two areas to allow discrimination.

2.4 GCaMP delivery to CLA

For *in vivo* studies, a retrograde viral strategy was used to deliver a calcium indicator specifically to the CLA. Three mice were injected with 100 nL of a retrograde AAV (Tervo et al., 2016) expressing Cre-recombinase (AAVrg-hSyn-Cre-WPRE-hGH; Addgene) in the RSC and 500 nL of AAV expressing Cre-dependent jGCaMP7b (AAV-syn-FLEX-jGCaMP7b-WPRE; Addgene).

2.5 Chronic window implantation

For chronic window and head-plate implantation a further surgery was needed. The procedure followed the same guidelines as detailed in a previous section for stereotaxic surgery, so here we only provide a summary of the relevant specific steps. First, a small portion of the scalp was removed around the window implantation site (over the prefrontal cortex). A 5 mm circular craniotomy was performed, centred on bregma. A partial durotomy was then performed, removing the dura covering the right hemisphere only. The window, formed of a 4 mm glass coverslip bonded to a 5 mm glass coverslip using optical cement (NOA61, Thorlabs), was inserted into the craniotomy hole. Mice were also implanted with a metal headplate with a 7 mm elliptical imaging well centred on the window. The head-plate and cranial window were sealed in place with Vetbond (3M) and dental cement (Super-Bond C&B, Sun-Medical).

2.6 Histology

Tissue collection for histological processing was only started once the animal was completely recovered from the surgery (at least five days) to allow enough time for the expression of viral vectors and retrograde labelling of the tracers. Cardiac arrest was induced by overdose with a fast acting barbiturate (Pentobarbital) administered i.p., followed by exsanguination with phosphate buffered saline (PBS) and perfusion through the left cardiac ventricle with 4% paraformaldehyde (PFA) for approximately one minute. Then, the brain was collected and fixation was completed at 4°C in 4% PFA overnight. Following, the brain was embedded in 4% agarose and sliced by vibratome (Leica CM3050s, Leica Biosystems) at ambient temperature to obtain 100 μm coronal sections. Slices were rinsed once in PBS for 5 minutes, stained with DAPI (1 $\mu\text{g}/\text{ml}$) in 0.1% Tween-20 PBS (PBST) for 10 minutes and washed twice in PBST for 5 minutes each. All this process was done in an orbital shaker (Stuart). Slices were mounted on microscope slides (Thermo Scientific), dried, gently impregnated in Fluoromount mounting medium (Sigma) and coverslipped. Images were acquired with an Olympus FV3000 confocal laser scanning microscope at 4x (numerical aperture 0.16) or 10x (numerical aperture 0.4) objective magnification (1-3x zoom). Images were processed with Olympus Fluoview software and ImageJ.

2.7 Steering wheel task set-up

The chosen behavioural paradigm was the steering wheel task which was initially set-up following its general-purpose description (Burgess et al., 2017) and by further indications by members of the Cortex Lab, UCL. Schematics, instructions and further documentation can be found at www.ucl.ac.uk/cortexlab/tools/wheel. Some components were 3D printed and some others bought from standard manufacturers.

During the task head-fixed mice are surrounded by three LCD monitors (refresh rate 60 Hz) located at both sides and in front of them and receive cue sounds from behind the screens. A photodiode was used to perform gamma correction of the screens. The

animal is located inside a plastic tube. The front paws of the animal were placed over a LEGO wheel with a rubber tire (62.4 mm in diameter). Mice were presented with stimuli consisting on vertical sinusoidal Gabor grids either in the left or right screen (azimuth 90°) and had to move the wheel to either the right or the left in self-learned movements in order to move the stimulus to the centre of the screen located in front of them. Movements of the wheel were tied to movements of the stimulus in the screen and measured by a rotary encoder (Kübler 05.2400.1122.0100). The rotary encoder had an approximate resolution of 0.9°, which corresponds to about 0.5 mm of the LEGO wheel circumference. A data acquisition device was used to integrate inputs and outputs from and to the task (National Instruments USB-6211).

In correct trials, water rewards were dispensed through a long metallic needle spout with small diameter (19 gauges), rubbed with teflon tape to avoid collapse of surface tension in the drop of water (i.e. to force water to form drops). Water delivery was controlled by a solenoid pump (Neptune Research 161T011) and the opening time of the valve was manually calibrated before each session to deliver precise volumes per reward.

The task was entirely controlled by MATLAB software using the open-source Signals package (github.com/dendritic/signals), and visual stimuli were presented through the Psychophysics Toolbox (Brainard, 1997; Pelli, 1997). The task was coordinated and designed with the Rigbox Toolbox (Bhagat et al., 2019). The main code for controlling the task was obtained from Burgess et al. (2017).

2.8 Training in the steering wheel task

Mice were placed on a water control schedule and given 40 ml/kg/day (which equals around 1 ml for the average 25g mouse). To monitor the effects of water restriction, during this period they were weighted daily and their weight was always maintained over 80% of their initial body mass. Signs of dehydration were also monitored: skin tension, sunken eyes, and marked variations in general behaviour (none of the mice showed

any of these signs). In order to avoid stress responses and stereotypic behaviour, when possible animals were co-housed with at least one same-sex littermate and guidelines were followed for cage environment enrichment (Würbel, 2001; Olsson and Dahlborn, 2002). Behavioural experiments were conducted in the evening. We did not investigate the effects of training at different times of the day in task performance.

Training procedure was gradual. Elements of the task were added and modified one at a time, as we found that modifying several elements at the same time confused the mice. The first two days of training mice were just handled for a time and head-fixed in the rig for 10 minutes without being presented any stimulus. This was to allow acclimatisation. After the acclimatisation period mice were trained in daily sessions of between 20 minutes and 1 hour. Initially, mice were trained with stimulus of 100% and 50% contrast and had no restriction in time to respond to each trial. The trial started with the presentation of the stimulus paired with a Go-Cue and finished when the stimulus azimuth reached 0° (front) or 180° (hypothetical back). In the first case mice were rewarded with 3 μ l of water; in the second case mice were presented with 0.5 seconds of a white noise burst.

The first step in the training process was that the mouse associated the movement of the wheel with the reward. To facilitate the association, in the first few sessions sometimes we would move the wheel if the mouse was inactive for a while or deliver water droplets to reward just the movement of the wheel. Once mice had learned to associate the movement of the wheel with the arrival of reward (ideally after one or two sessions) mice were left completely on their own to perform the task. Along trials the sensitivity of the wheel with respect to the movement of the stimulus in the screen was adjusted so that it would be optimal for the learned movements of each mouse (initially a 45° turn of the wheel would result in a displacement of the azimuth for the stimulus of 90°). If a mouse was responding much better to a stimulus presented on one of the screens (i.e. if there was a clear tendency to move the wheel only in one direction), in the next session we presented more stimuli in one of the sides so that the mouse would be forced to move the wheel to the 'non-dominant' direction. Initially, wrong trials were forced to be repeated until the

mouse performed correctly.

Once their performance was over 70%, parameters started to be modified in order to add complexity to the task. If performance was maintained or improved, further modifications of the trials were made in the following sessions. First, reward size was reduced to $2.5 \mu\text{l}$ per correct trial, in order to increase the number of trials mice did per session. Then a quiescent period of 0.2 seconds was introduced at the beginning of each trial. During this time the mouse should not move the wheel. If the animal made a movement during this time the quiescent time counter was re-initialised and the quiescent period started again until full completion. This was introduced so that mice will stop moving the wheel after the trial was completed. Next, a 0.5 second open loop was introduced between the quiescent period and the trial. During this time the stimulus appeared in the screens but the movement of the wheel was not tied to it. This was introduced to dissociate motor activity from sensory stimulation. Mice tended to hold the wheel still during this period. Then we introduced an 8 seconds response window (closed loop period). If mice did not respond to stimuli presented in that range of time, a 0.5 seconds white noise burst was presented and the next trial initiated. At this point we lowered the reward to its final value, $2 \pm 0.2 \mu\text{l}$ per trial, and the closed loop to 1.5 seconds. Both decays were made progressively across a number of sessions. Because at this point trials were rapidly following one to the other, we believed it convenient to introduce a delay of 2 seconds between trials (also introduced progressively). Another reason why we introduced this inter-trial delay was so that during imaging experiments we could easily separate responses to different elements of the task (e.g. reward delivery and visual stimulus presentation). At this point we eliminated the repetition of incorrect trials and changed reward for 10% sucrose in water, which was more appealing to the mice and resulted in a big increase in the number of trials made per session. Finally, No-Go trials were introduced in one-third of the trials. In these ones, there was a go cue at the beginning of the trial but no stimulus was presented in any of the screens. Mouse had to hold still the wheel for the duration of the trial to be rewarded. Small movements of the wheel

were not penalised, but if the movement was significant (similar to the one they will do in a Go trial) they were presented with 0.5 seconds of a white noise burst. Initially they had to repeat failed No-Go trials. After a number of sessions (around five sessions), once they had learned this contingency repetitions were eliminated.

To calculate the performance in each session we only considered completed trials (i.e. when the mouse had responded, including holding the wheel still during a No-Go trial) and only the first trial if the repetition of wrong trials was taking place. Trials in which the stimulus were presented but the mouse did not respond were considered missed trials. The ratio of correct versus incorrect trials defined the performance of the session. We did not consider more complex psychometric functions as stimuli were only presented at 50 or 100% contrast (Burgess et al., 2017).

2.9 Whisker stimulation

For examining claustrum responses to somatosensory stimulation one mouse was head-fixed and its left whiskers were stimulated at a frequency of 20 Hz for one second, every 10 seconds, for 2 and a half minutes (20 presentations in total) while performing two-photon calcium imaging. Whiskers were stimulated with a custom paddle connected to a 3–16V continuous interval piezo buzzer (RS Components 511-7636). This experiment was repeated in three different fields of view in the right hemisphere. Unfortunately, we are unsure about the precise location where we imaged, most likely the rostral part of the retrosplenial cortex or more frontal regions along the midline.

2.10 Two-photon imaging in the awake mouse

For imaging during the steering wheel task, mice were trained in the microscope set-up for three days prior to the imaging experiment to acclimatise them to the new environment. For imaging during whisker stimulation mice were not acclimated. Two-photon imaging

of jGCaMP7b was performed using a customized Bruker 2P-Plus with a Chameleon Vision-S (Pulse width 75 fs; Coherent) at 920 nm. The beam power for the Chameleon Vision-S was controlled using a Pockels cell (Conoptics Ltd.). Imaging was performed through a 16 X water immersion objective lens (numerical aperture 0.8; Nikon) with a power on sample of 50 to 80 mW. Fluorescence time-series were recorded between 100 and 400 μ m deep at a frame rate of 30 Hz (Field of view 512 x 512 μ m). PackIO open-source software (Watson et al., 2016) was used to synchronise recordings with elements of the steering wheel task (e. g. reward delivery) or, in the case of the whisker stimulation experiment, with the onset of each stimulation. When imaging during the steering wheel task we had to deal with an added complication: the light coming from the screens into the imaging objective saturated the photomultipliers. To overcome this difficulty we created a light blocking shield around the objective. We glued a black silicon ring to the head-plate of the animal and applied a silicone elastomer (KWIK-SIL, World Precision Instruments) around its edges to seal it and prevent water in the objective-window interface from escaping. The interface was then completely enclosed with a loose sleeve made with several layers of foil and black electrical tape. This solution was not optimal because it interfered in the movement of the microscope in the z axis, was difficult to set up in each session and did not completely block all the light. In the future a more refined solution should be used.

2.11 Axonal calcium imaging analysis

Suite2p Python package was used to semi-automatize processing of axonal calcium imaging data time-series (Pachitariu et al., 2017). Suite2p is an optimal package to analyse data from somatic calcium imaging experiments but can also be used for axonal imaging. The processing flow includes registration of the stack, finding regions of interest (ROIs), classifying ROIs as cells or non-cells and extracting and deconvolving fluorescent traces from the ROIs. We optimised the hyperparameters of the software in order to adapt the programme to our needs. In particular, by disabling a ROI pre-processing algorithm the

programme was able to find axons, which had to be later curated by hand. The change in fluorescence was calculated as follows:

$$\frac{dF}{F} = \frac{F - \tilde{F}}{\tilde{F}} \quad (1)$$

Where \tilde{F} is the median of F , the raw fluorescent trace, over the whole recording. We calculated the stimulus triggered average (STA) for each ROI as the mean dF/F signal at each time point across trials, 3 seconds before and after the stimulus. All the code for analysis and plotting was written in Python and is available at a public repository:

<https://github.com/diegoasua/CLA-analysis.git>

3 Results

3.1 Projection-defined CLA neurons

We first investigated two potential candidate areas to which the CLA is known to project: ACA and RSC. To assess the specificity and strength of retrograde labelling from these areas to the CLA we injected a retrograde anatomical tracer, Cholera Toxin subunit B (CTB), fused to an Alexa fluorophore unilaterally in both areas of the same animal. This would allow us to compare the extent of labelling and the overlap in CLA-projecting neurons (Figure 1A). CTB crosses cellular membranes and travels backwards from axonal and dendritic terminals to soma (Luppi et al., 1990).

We injected ten mice with this strategy. Five surgeries were unsuccessful. Of the remaining five, four had good labelling of the ACA but no labelling from the RSC and one had good labelling from the RSC but no labelling from the ACA. In Figure 1B we show the only successful RSC injection and in Figure 1C one representative successful ACA injection.

Because of this limitation, here we simply qualitatively compare the extent of labelling along the antero-posterior axis of RSC and ACA-projecting CLA neurons in two different animals (Figure 1B-E). Both strategies strongly labelled the CLA along its length, meaning that the CLA extensively and strongly projects to these two areas. However, RSC-projecting CLA was spatially more confined, especially in the more rostral parts of the extended CLA sheet. This was consistent in the four animals injected into the ACA. The wider spread of ACA-defined CLA-projecting neurons meant that some cells from the nearby insular or piriform cortices may have been labelled, although in any case very few. We also found a large extent of labelling in the caudoputamen and thalamus, as well as several cortical areas.

Although Zingg et al. (2018) claim that retrograde labelling from the RSC is more specific

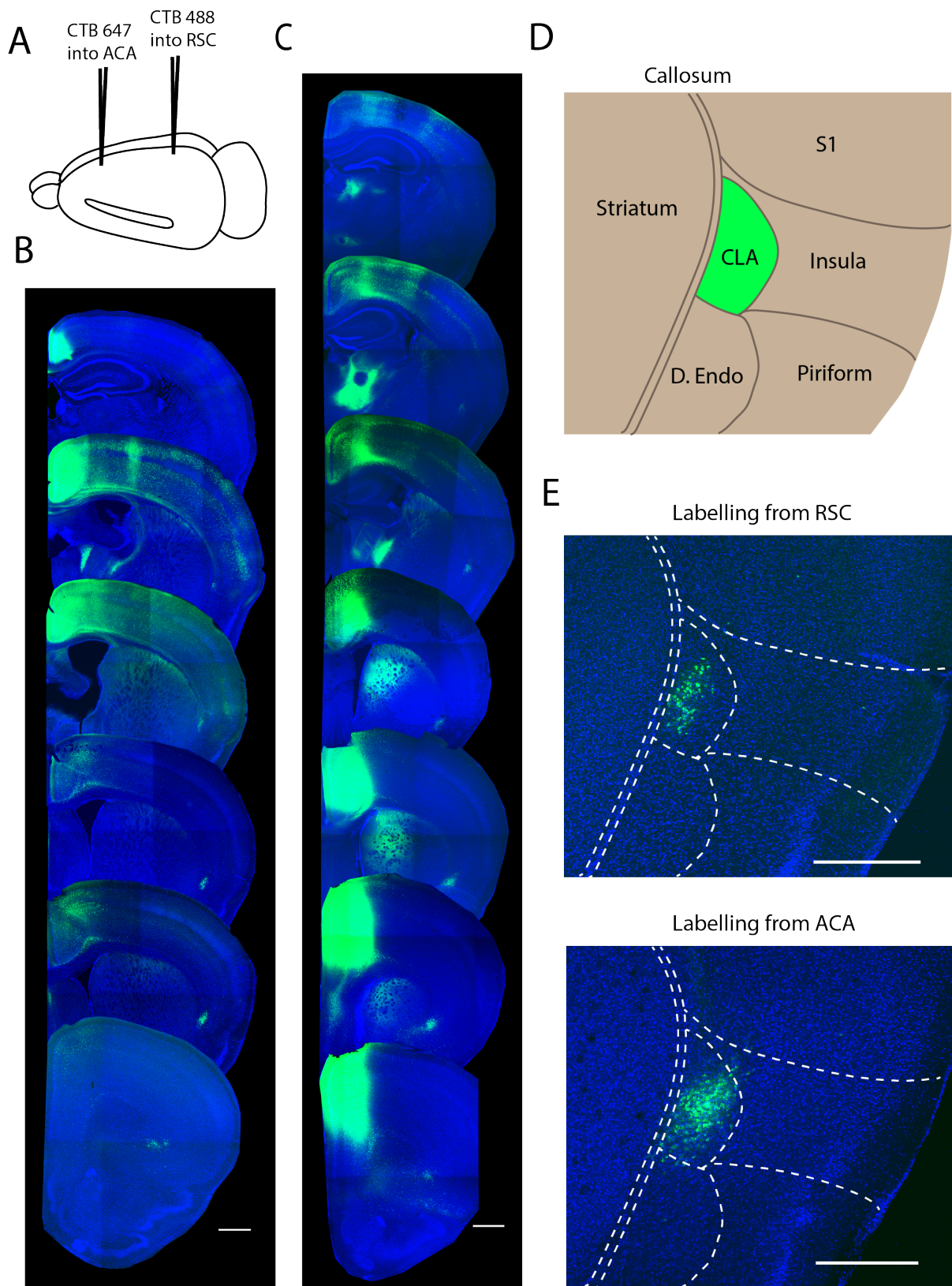


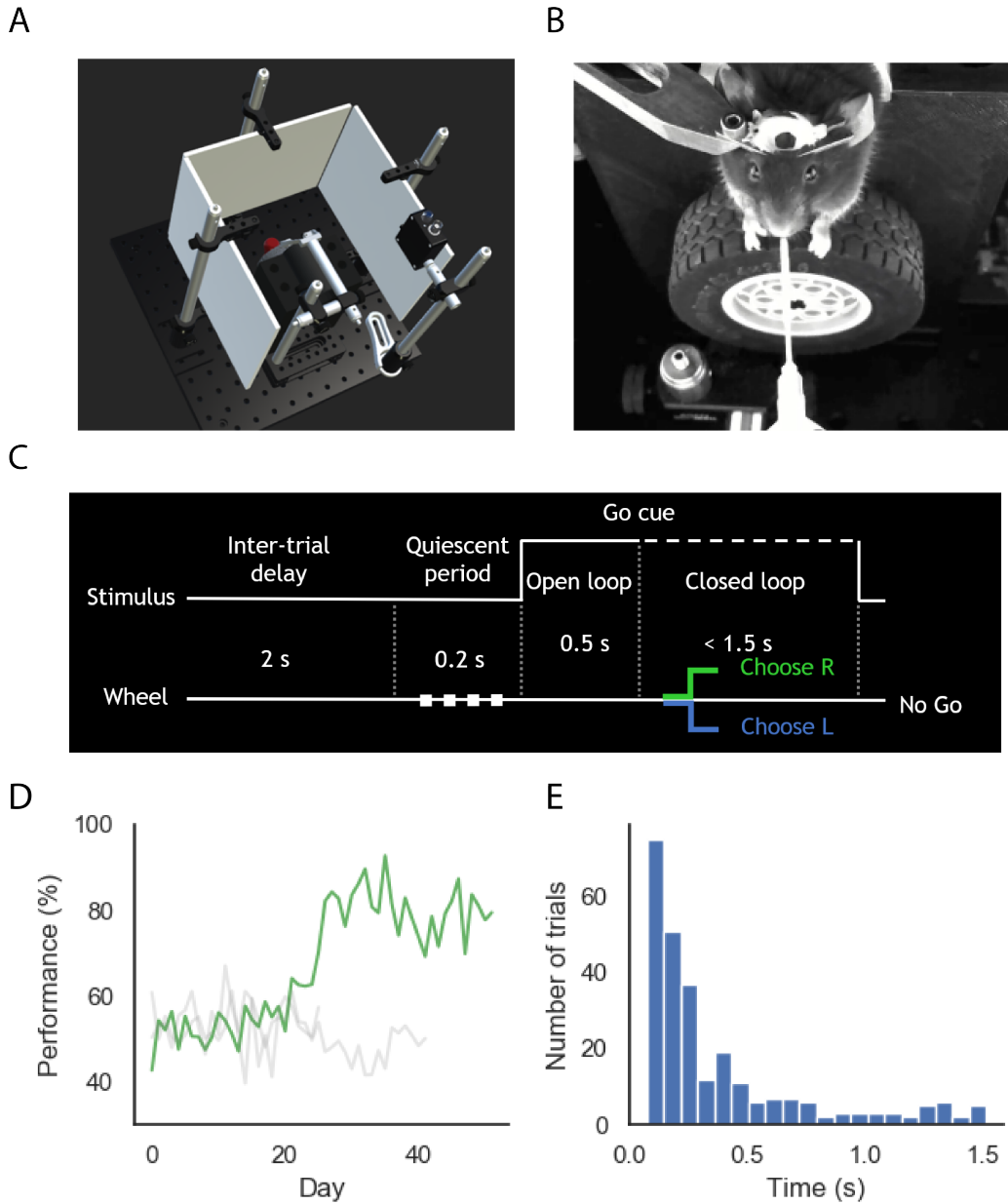
Figure 1: Retrograde CTB labelling of the CLA along the rostro-caudal axis. Blue: DAPI; Green: CTB-Alexa. (A) Schematic showing the injection strategy (B) CTB labelling from RSC. (C) CTB labelling from ACA. (D) Location of the CLA in a coronal section (around 0.345 mm posterior to bregma according to the Allen Reference Atlas). (E) Alignment of the corresponding coronal slice with the Atlas shown in (D). Scale bar is 1 mm in B and C and 500 μ m in E. S1: primary somatosensory cortex; D. Endo: Dorsal endopiriform nucleus; CLA: Claustrum.

and less prompt to lead to off-targets than labelling from the ACA, here we conclude that both RSC and ACA are good candidates for the use of a retrograde viral strategy targeting the CLA. Nevertheless, we acknowledge that this conclusion is drawn from just one successful RSC injection. Repeating the experiment in more animals should show whether this finding is consistent.

3.2 A behavioural scenario to probe the CLA

In order to probe CLA function we need a behavioural task involving different discriminable cognitive functions. Hypothetically, we could subject mice to a battery of tests while recording activity from the CLA and observe elements of such tests (e.g. sensory stimuli) that evoke activity (e.g. calcium transients). However, this would take too long and would require setting up a number of tasks, which is far from ideal. Luckily however, the Cortex lab in UCL has recently developed a complex quantitative behavioural task that requires motor learning, visuomotor integration, attention, working memory and the reward system, known as the steering wheel task (Figure 2A-C) (Burgess et al., 2017). Moreover, the task is highly modular and adaptable, and can be modified, for example, to include multisensory integration (Coen et al., 2018). This task is optimal for studying CLA function because it combines a battery of cognitive functions which, due to the structure of the task, can be assessed independently.

We built a steering wheel set-up in which head-fixed mice were presented with stimuli in the form of sinusoidal gratings on either their right or their left. Their task was to move a wheel in the required direction so that the stimulus would end up in front of them. For each trial in the task, if they succeeded, they were given a liquid reward, whereas moving the wheel in the wrong direction was punished with a white noise burst time-out. Mice were trained in a simple, two alternative forced-choice version of the task. Complexity was gradually introduced into the task to give rise to an unforced-choice visuomotor task guided by auditory Go-Cues (Figure 2C). In this final version of the steering wheel task,



mouse had to hold still the wheel for 0.2 seconds. Then they were presented with the stimulus for 0.5 seconds (open loop period), during which movements of the wheel were not tied to movements of stimulus in the screen. Then an auditory Go cue was presented and mice had 1.5 seconds to make a choice – right or left (closed loop period). During No-Go trials the structure was the same but no stimulus was presented in the screens. Mice had to hold the wheel still. Two seconds of delay separated one trial from the next.

We trained three mice in the task. Only one animal managed to learn the task in its entire complexity, whereas the other two performed at chance (Figure 2D). This was most probably caused by technical difficulties that arose from setting up the task during the first three weeks of training, and which likely confused mice. After overcoming these initial troubles, a mouse learnt the unforced-choice version of the task and reached a steady performance of over 80% in less than 30 days of training. Once trained the median response time of the mouse was 0.2 seconds (Figure 2E).

3.3 Imaging during the steering wheel task

Because the CLA is deep into the neocortex – around 900 μm beyond the cortical surface in its closest point along the rostro-caudal axis – direct two-photon imaging is nearly impossible with current scope of optical technologies. However, because the CLA densely projects to many cortical areas (Torgerson et al., 2014; Wang et al., 2019; Zingg et al., 2018) we can, instead, record axonal responses from claustrocortical collaterals in different regions of cortex as a way to record its activity.

Following this reasoning, we delivered to the CLA a genetically encoded bright calcium indicator – jGCaMP7b – which is optimal for recording axonal and dendritic calcium transients *in vivo* (Dana et al., 2018). We accomplished this by taking advantage of the specificity of RSC-defined projecting neurons. Briefly, a Cre-expressing tailored AAV variant that travels retrogradely (Tervo et al., 2016) was injected into the RSC and a Cre-dependent, FLEX-ed jGCaMP7b expressing AAV was injected directly into the

CLA (Figure 3A). Through this strategy we were able to deliver the calcium indicator exclusively to our target with minimal number of off-target cells labelled (Figure 3B-C). The calcium indicator was found both in the soma and dendritic and axonal projections (Figure 3C). A cranial window was implanted over the prefrontal cortex (PFC) to image axons coming from these neurons (Figure 3A).

We then performed *in vivo* two-photon imaging of axons in several field of views (FOVs) along layers 2, 3 and 4 of PFC in one trained mouse performing the steering wheel task. We selected FOVs in which we could see a high rate of activity. We could only identify a small number of axons in each FOV (Figure 3D-E). This was most probably because at the time of recording the animal had been injected with the calcium indicator several months before. We measured changes in fluorescence of jGCaMP7b to determine the activity of each identified axon and built stimulus-triggered averages (STAs) around the open loop period and the delivery of a reward following a correct trial (Figure 3F-G). In some – just a small number – of the trials, some axons (e.g. the one shown in Figures 3F and 3G, left) showed dF/F transients immediately after the open-loop or the delivery of reward, but this was not consistent across a large number of trials. This indicated that none of the recorded axons were tied to either the onset of reward or the presentation of the visual stimulus. These results have to be taken with extreme precaution due to a number of factors: 1) The experiment was only carried out in one animal; 2) The calcium indicator was delivered months before the actual recording. Prolonged expression of the genetically encoded calcium indicator may have caused neurotoxicity. 3) Only a small number of axons were recorded. 4) The signal-to-noise ratio in most recordings was very low.

3.4 CLA axonal responses to somatosensory stimulation

Several studies have described that the CLA responds to stimuli in different sensory modalities (Olson and Graybiel, 1980; Remedios et al., 2010). In particular, previous

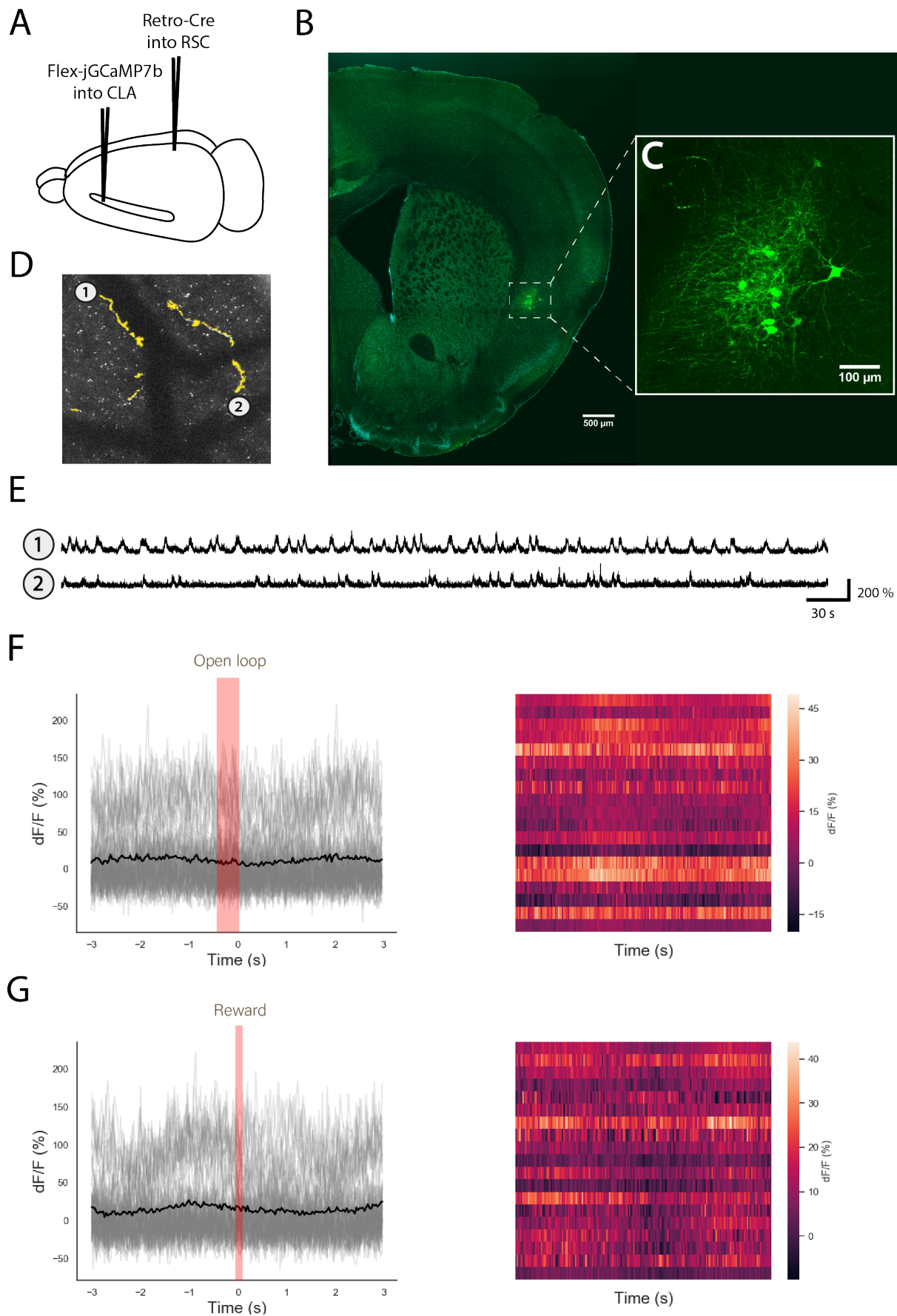


Figure 3: Two-photon axonal calcium imaging in the steering wheel task. (A) Schematic showing the injection strategy used to deliver a calcium indicator specifically to the claustrum. (B) A representative coronal section showing jGCaMP7b only in the CLA (green). Scale bar is 500 μ m. (C) Detail of CLA cells showing somas, dendrites and axons with jGCaMP7b. (D) Example *in vivo* field of view recorded during the steering wheel task. Detected axons are coloured in yellow (E) dF/F traces for 10 minutes of recording corresponding to axons shown in D. Scale bar is 30 seconds and 200% dF/F. (F) Left: Stimulus-triggered average (STA) of the dF/F signal of an example axon around the open-loop period of the steering wheel task. In grey, individual trials, in black, STA trace. Red area shows the duration of the open loop. Right: Heatmap for the STA of a number of recorded axons in several field of views centred around the open-loop. Colour scale represents dF/F. (G) Same as F but centred around the reward in the steering wheel task.

results from our research group indicated that claustrum axons – or at least a subset of them – respond to the presentation of auditory stimuli (Oliver, 2019). Following these exciting results, we expected axons from the CLA to also generate calcium transients in response to somatosensory stimulation.

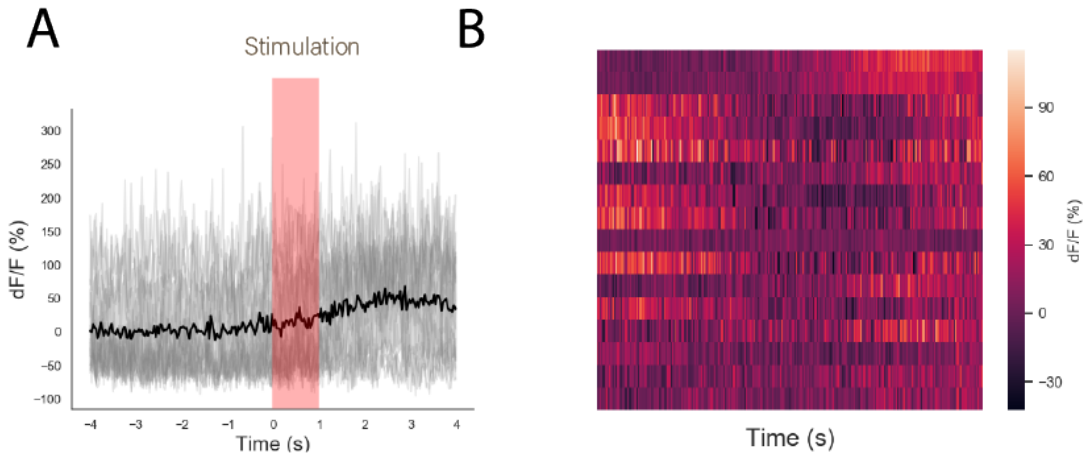


Figure 4: Two-photon axonal calcium imaging during whisker stimulation. (A) Stimulus-triggered average of dF/F signal of an example axon around the onset of stimulation. In grey, individual trials, in black, STA trace. Red area shows the duration of the stimulus. (B) Heatmap for the STA of a number of recorded axons in several field of views centred around stimulus onset. Colour scale represents dF/F..

We imaged CLA axons in the right PFC layers 2, 3 and 4 of one animal – different from the animal used for the steering wheel task – while bulk stimulating with a mechanical piezo his left whiskers for 1 second trials in intervals of 10 seconds. We analysed the acquired data as described in the previous section and found a modest increase in dF/F signal in some recorded axons overlapping with the presentation of the stimulus (Figure 4A-B). However, taking the representative example in Figure 4A, the STA clearly shows that the increase of fluorescence started some hundreds of milliseconds before the onset of stimulation. This may suggest that the recorded axons were just firing according to a

rate which in some cases happened to partially overlap with the regularly spaced timing of the presentation of the stimulus.

4 Discussion

This study has reported axonal calcium imaging of CLA collaterals in mice performing a complex sensorimotor task and during somatosensory stimulation. Here we have first investigated the extent of overlap between CLA neurons projecting to either the RSC or the ACA. Based on the results shown here, previous results from our research group (Oliver, 2019) and from published experiments (Wang et al., 2017; Zingg et al., 2018) we have noted that retrograde tracing from RSC is an optimal strategy to define the CLA with minimal off-target effects. Taking advantage of this, we have unilaterally expressed *jGCaMP7b* specifically in the CLA of mice, trained them in a sensory-guided task that requires motor skills and imaged collaterals from this structure in the PFC during behaviour.

Although CLA projects to a myriad of cortical structures, so do the nearby insular and endopiriform cortices. Here we have shown that ACA and RSC-projecting neurons are found in the CLA in all its rostro-caudal axis – which extends around 3 mm in the mouse brain – but do not seem to cover the insula or endopiriform nucleus. Unfortunately, we could not investigate the extent of overlap between CLA neurons with projection targets in the RSC and those with projection targets in the ACA. This was due to failure of the double injection strategy. The candidate did make progress in this technique during the project, as seen by the increase in the number of successful injections at the end of the project compared to the start; however, owing to the limited duration of this project we could not inject a further number of animals.

It took around fifty days to successfully train one animal in the steering wheel task. In the original description of the task mice took between four and five weeks of training to get to a good performance stage in a similar paradigm to the one used here (Burgess et al., 2017). In our hands, it took around three weeks to set-up and optimise the task, which is why we observe such a delay in the amount of days required for training and the training yield (one out of three animals). Technical difficulties arose along those three

weeks that complicated the training process and confused the mice, such as problems with screen resolution, the licking and pumping systems and even the position of the mouse over the wheel. Interestingly, we noticed this last variable is one of the most influential in the task and can be very variable depending on the head-fixing apparatus. A good habit for overcoming this difficulty is taking a picture of each animal once is head-fixed and comparing them across days to ensure that the position of the animal remains the same.

In vivo functional recordings of axonal activity under sensory stimulation have been already reported multiple times (Petreanu et al., 2012; Wilms and Häusser, 2015). One paper imaged calcium transients from hippocampal CA1 axons and dendrites in mice navigating through a virtual maze (Sheffield and Dombeck, 2014), but to the best of our knowledge no other report than this one and the present have imaged axonal calcium responses in behaving animals on any task that require plenty of motor activity. Axonal imaging in the behaving mouse is challenging because of the ease with which axons may get out of the focal plane due to movement, especially in scenarios that require plenty of motor activity such as the steering wheel task. A recent study has implicated the claustrum in reward acquisition (White et al., 2018b). However, here we found no correlation between reward timing in the steering wheel task and the onset of calcium transients in recorded claustrocortical collaterals, which suggests that the CLA is indeed not involved in reward acquisition according to our study. We did not find either a correlation with visual stimulus presentation in the steering wheel task and only a weak correlation with whisker stimulation alone. This was surprising as the CLA has been repeatedly shown to respond to sensory stimulation in different sensory modalities (Remedios et al., 2010, 2014; Atlan et al., 2018). Moreover, auditory and visual cortical areas as well as whisker-related motor cortical areas project to the CLA (Wang et al., 2017; Smith and Alloway, 2010). One explanation for this may be that we were recording from CLA collaterals involved in other functions, but not in these ones. Mice were old and had been injected months ago at the time of imaging, and we observed very little number of axons in each

of our FOVs, suggestive of some kind of axon degeneration, probably related to prolonged GCaMP expression, which has been shown to be neurotoxic in the long term (Tian et al., 2009). Therefore it could be that the observed activity corresponds only to a subset of axons

Due to the depth at which the CLA is located in the mouse brain, which makes it nearly impossible to be imaged with standard state of the art two-photon imaging, this study is limited to recording calcium activity from axons crossing or ending in cortical areas. Further studies may be able to record directly from the claustrum by using three-photon calcium imaging in behaving mice (Horton et al., 2013; Wang et al., 2018).

Conclusion

It is most likely that the claustrum plays a central role in integrating cortical information. However, its role is still an enigma for the neuroscientific community. Calcium imaging, and in particular axonal calcium imaging in the behaving mouse has opened the door to probing several candidate functions for the claustrum. Here, by using this technique we did not find any clear correlation between axonal activity from the claustrum and reward acquisition or visual or somatosensory stimulation. However, this is a pilot study and these findings should be further confirmed and explored with a bigger cohort and more rigorous experimental conditions. We foresee calcium imaging in the behaving mouse as a valuable tool that may one day uncover the many mysteries of the claustrum.

5 References

- Atlan, G., Terem, A., Peretz-Rivlin, N., Sehrawat, K., Gonzales, B. J., Pozner, G., Tasaka, G.-i., Goll, Y., Refaeli, R., Zviran, O., Lim, B. K., Groysman, M., Goshen, I., Mizrahi, A., Nelken, I., and Citri, A. (2018). The Claustrum Supports Resilience to Distraction. *Current Biology*, 28:2752–2762.
- Bayat, A., Joshi, S., Jahan, S., Connell, P., Tsuchiya, K., Chau, D., Syed, T., Forcelli, P., and Koubeissi, M. Z. (2018). A pilot study of the role of the claustrum in attention and seizures in rats. *Epilepsy Research*, 140:97–104.
- Binks, D., Watson, C., and Puelles, L. (2019). A Re-evaluation of the Anatomy of the Claustrum in Rodents and Primates—Analyzing the Effect of Pallial Expansion. 13:1–11.
- Burgess, C. P., Lak, A., Steinmetz, N. A., Zatka-Haas, P., Bai Reddy, C., Jacobs, E. A. K., Linden, J. F., Paton, J. J., Ranson, A., Schröder, S., Soares, S., Wells, M. J., Wool, L. E., Harris, K. D., and Carandini, M. (2017). High-Yield Methods for Accurate Two-Alternative Visual Psychophysics in Head-Fixed Mice. *Cell Reports*, 20:2513–2524.
- Coen, P., Wells, M. J., Myers-Joseph, D., Carandini, M., and Harris, K. D. (2018). Cortical basis of audiovisual spatial localization in mouse. In *Society for Neuroscience Annual Meeting*.
- Crick, F. and Koch, C. (2005). What is the function of the claustrum? *Philosophical Transactions of the Royal Society B: Biological Sciences*, 360:1271–1279.
- Dana, H., Sun, Y., Mohar, B., Hulse, B., Hasseman, J. P., Tsegaye, G., Tsang, A., Wong, A., Patel, R., Macklin, J. J., Chen, Y., Konnerth, A., Jayaraman, V., Looger, L. L., Schreiter, E. R., Svoboda, K., and Kim, D. S. (2018). High-performance GFP-based calcium indicators for imaging activity in neuronal populations and microcompartments. *bioRxiv*.

- Dillingham, C. M., Mathiasen, M. L., Frost, B. E., Lambert, M. A. C., Bubb, E. J., Jankowski, M. M., Aggleton, J. P., and O'Mara, S. M. (2019). The Anatomical Boundary of the Rat Claustrum. *Frontiers in Neuroanatomy*, 13:1–17.
- Fernández-Miranda, J. C., Rhiton, A. L., Kakizawa, Y., Choi, C., and Álvarez-Linera, J. (2008). The claustrum and its projection system in the human brain: a microsurgical and tractographic anatomical study. *Journal of Neurosurgery JNS*, 108:764–774.
- Goldowitz, D. (2010). Allen Reference Atlas. A Digital Color Brain Atlas of the C57BL/6J Male Mouse - by H. W. Dong. *Genes, Brain and Behavior*, 9:128.
- Horton, N. G., Wang, K., Kobat, D., Clark, C. G., Wise, F. W., Schaffer, C. B., and Xu, C. (2013). In vivo three-photon microscopy of subcortical structures within an intact mouse brain. *Nature Photonics*, 7:205–209.
- Jackson, J., Karnani, M. M., Zemelman, B. V., Burdakov, D., and Lee, A. K. (2018). Inhibitory Control of Prefrontal Cortex by the Claustrum. *Neuron*, 99:1029–1039.
- Johnson, J. I. and Fenske, B. A. (2014). The claustrum: Structural, functional and clinical Neuroscience. pages 1–27. Academic Press, San Diego.
- Kennedy, H. and Bullier, J. (1985). A double-labeling investigation of the afferent connectivity to cortical areas V1 and V2 of the macaque monkey. *The Journal of Neuroscience*, 5:2815–2830.
- Krimmel, S. R., White, M. G., Panicker, M. H., Barrett, F. S., Mathur, B. N., and Seminowicz, D. A. (2019). Resting state functional connectivity and cognitive task-related activation of the human claustrum. *NeuroImage*, 196:59–67.
- LeVay, S. and Sherk, H. (1981). The visual claustrum of the cat. I. Structure and connections. *The Journal of Neuroscience*, 1:956–980.
- Luppi, P.-H., Fort, P., and Jouvet, M. (1990). Iontophoretic application of unconjugated cholera toxin B subunit (CTb) combined with immunohistochemistry of neurochemical

- substances: a method for transmitter identification of retrogradely labeled neurons. *Brain Research*, 534:209–224.
- Majak, K., Pikkarainen, M., Kemppainen, S., Jolkonen, E., and Pitkänen, A. (2002). Projections from the amygdaloid complex to the claustrum and the endopiriform nucleus: A Phaseolus vulgaris leucoagglutinin study in the rat. *Journal of Comparative Neurology*, 451:236–249.
- Mathur, B. N., Caprioli, R. M., and Deutch, A. Y. (2009). Proteomic Analysis Illuminates a Novel Structural Definition of the Claustrum and Insula. *Cerebral Cortex*, 19:2372–2379.
- Narikiyo, K., Mizuguchi, R., Ajima, A., Mitsui, S., Shiozaki, M., Hamanaka, H., Johansen, J. P., Mori, K., and Yoshihara, Y. (2018). The Claustrum Coordinates Cortical Slow-Wave Activity. *bioRxiv*.
- Oliver, D. (2019). *Optical methods for in vivo recording and manipulation of the mouse claustrum*. Msc dissertation, University of Oxford.
- Olsson, C. R. and Graybiel, A. M. (1980). Sensory maps in the claustrum of the cat. *Nature*, 288:479–481.
- Olsson, I. A. O. and Dahlborn, K. (2002). Improving housing conditions for laboratory mice: a review of 'environmental enrichment'. *Laboratory Animals*, 36:243–270.
- Pachitariu, M., Stringer, C., Dipoppa, M., Schröder, S., Rossi, L. F., Dalgleish, H., Carandini, M., and Harris, K. D. (2017). Suite2p: beyond 10,000 neurons with standard two-photon microscopy. *bioRxiv*.
- Pearson, R. C. A., Brodal, P., Gatter, K. C., and Powell, T. P. S. (1982). The organization of the connections between the cortex and the claustrum in the monkey. *Brain Research*, 234:435–441.
- Petreanu, L., Gutnisky, D. A., Huber, D., Xu, N.-l., O'Connor, D. H., Tian, L., Looger,

- L., and Svoboda, K. (2012). Activity in motor–sensory projections reveals distributed coding in somatosensation. *Nature*, 489:299–306.
- Remedios, R., Logothetis, N., and Kayser, C. (2014). A role of the claustrum in auditory scene analysis by reflecting sensory change. *Frontiers in Systems Neuroscience*, 8:1–8.
- Remedios, R., Logothetis, N. K., and Kayser, C. (2010). Unimodal Responses Prevail within the Multisensory Claustrum. *The Journal of Neuroscience*, 30:12902–12907.
- Renouard, L., Billwiller, F., Ogawa, K., Clément, O., Camargo, N., Abdelkarim, M., Gay, N., Scoté-Blachon, C., Touré, R., Libourel, P.-A., Ravassard, P., Salvert, D., Peyron, C., Claustrat, B., Léger, L., Salin, P., Malleret, G., Fort, P., and Luppi, P.-H. (2015). The supramammillary nucleus and the claustrum activate the cortex during REM sleep. *Science Advances*, 1:e1400177.
- Sheffield, M. E. J. and Dombeck, D. A. (2014). Calcium transient prevalence across the dendritic arbour predicts place field properties. *Nature*, 517:200–215.
- Sherk, H. (2014). The claustrum: Structural, functional and clinical Neuroscience. pages 177–191. Academic Press, San Diego.
- Smith, J. B. and Alloway, K. D. (2010). Functional specificity of claustrum connections in the rat: interhemispheric communication between specific parts of motor cortex. *The Journal of neuroscience*, 30:16832–16844.
- Tervo, D., Hwang, B.-Y., Viswanathan, S., Gaj, T., Lavzin, M., Ritola, K., Lindo, S., Michael, S., Kuleshova, E., Ojala, D., Huang, C.-C., Gerfen, C., Schiller, J., Dudman, J., Hantman, A., Looger, L., Schaffer, D., and Karpova, A. (2016). A Designer AAV Variant Permits Efficient Retrograde Access to Projection Neurons. *Neuron*, 92:372–382.
- Tian, L., Hires, S. A., Mao, T., Huber, D., Chiappe, M. E., Chalasani, S. H., Petreanu, L., Akerboom, J., McKinney, S. A., Schreiter, E. R., Bargmann, C. I., Jayaraman, V.,

- Svoboda, K., and Looger, L. L. (2009). Imaging neural activity in worms, flies and mice with improved GCaMP calcium indicators. *Nature Methods*, 6:875–884.
- Torgerson, C. M., Irimia, A., Goh, S. Y. M., and Van Horn, J. D. (2014). The DTI connectivity of the human claustrum. *Human Brain Mapping*, 36:827–838.
- Wang, Q., Ng, L., Harris, J. A., Feng, D., Li, Y., Royall, J. J., Oh, S. W., Bernard, A., Sunkin, S. M., Koch, C., and Zeng, H. (2017). Organization of the connections between claustrum and cortex in the mouse. *Journal of Comparative Neurology*, 525:1317–1346.
- Wang, T., Ouzounov, D. G., Wu, C., Horton, N. G., Zhang, B., Wu, C.-H., Zhang, Y., Schnitzer, M. J., and Xu, C. (2018). Three-photon imaging of mouse brain structure and function through the intact skull. *Nature Methods*, 15:789–792.
- Wang, Y., Xie, P., Gong, H., Zhou, Z., Kuang, X., Wang, Y., Li, A.-a., Li, Y., Liu, L., Veldman, M. B., Daigle, T. L., Hirokawa, K. E., Qu, L., Lesnar, P., Jiang, S., Yu, Y., Wakeman, W., Zeng, S., Li, X., Yuan, J., Nguyen, T. N., Larsen, R., Kebede, S., Song, Y., Yin, L., Zhao, S., Feiner, A., Shen, E., Hill, C., Wang, Q., Mok, S., Sunkin, S. M., Josh Huang, Z., Esposito, L., Yao, Z., Hawrylycz, M. J., Tasic, B., Ng, L., Sorensen, S. A., William Yang, X., Harris, J. A., Koch, C., Luo, Q., Peng, H., and Zeng, H. (2019). Complete single neuron reconstruction reveals morphological diversity in molecularly defined claustral and cortical neuron types. *bioRxiv*.
- Watakabe, A., Ohsawa, S., Ichinohe, N., Rockland, K. S., and Yamamori, T. (2014). Characterization of claustral neurons by comparative gene expression profiling and dye-injection analyses . *Frontiers in Systems Neuroscience*, 8:1–14.
- Watson, B. O., Yuste, R., and Packer, A. M. (2016). PackIO and EphysViewer: software tools for acquisition and analysis of neuroscience data. *bioRxiv*.
- White, M. G., Mu, C., Zeng, H., and Mathur, B. N. (2018a). The claustrum is required for reward acquisition under high cognitive demand. *bioRxiv*.

- White, M. G., Panicker, M., Mu, C., Carter, A. M., Roberts, B. M., Dharmasri, P. A., and Mathur, B. N. (2018b). Anterior Cingulate Cortex Input to the Claustrum Is Required for Top-Down Action Control. *Cell Reports*, 22:84–95.
- Wilms, C. D. and Häusser, M. (2015). Reading out a spatiotemporal population code by imaging neighbouring parallel fibre axons in vivo. *Nature Communications*, 6:1–9.
- Würbel, H. (2001). Ideal homes? Housing effects on rodent brain and behaviour. *Trends in Neurosciences*, 24:207–211.
- Zingg, B., Dong, H.-W., Tao, H. W., and Zhang, L. I. (2018). Input–output organization of the mouse claustrum. *Journal of Comparative Neurology*, 526:2428–2443.